Mass Spectrometry Evidence for Self-Rigidification of π-Conjugated Oligomers Containing 3,4-Ethylenedioxythiophene (EDOT) Groups using RRKM Theory and Internal Energy Calibration

David Rondeau, Yves Gimbert, Karoly Vekey, Laszlo Drahos, Mathieu Turbiez, Pierre Frère, Jean Roncali

Mass Spectrometry Evidence for Self-Rigidification of π-Conjugated Oligomers Containing 3,4-Ethylenedioxythiophene (EDOT) Groups using RRKM Theory and Internal Energy Calibration

David Rondeau*,[a,b] Yves Gimbert,[c] Károly Vékey,[d] Laszlo Dráhos,[d] Mathieu Turbiez,[e] Pierre Frère[e] and Jean Roncali[e]

[a] Université de Rennes 1, Institute d'Electronique et de Télécommunications de Rennes IETR UMR CNRS 6164, Campus de Beaulieu, 263 avenue du Général Leclerc, 35042 Rennes Cedex, France.

[b] Univ. Grenoble Alpes and CNRS, DCM (UMR 5250) BP 53,

38041 Grenoble Cedex9 France

[c] Université de Bretagne Occidentale, Département de Chimie, 6 avenue Victor Le Gorgeu, 29238 Brest, Cedex, France.

[d] MS Proteomics Research Group, Research Centre for Natural Sciences, Hungarian Academy of Sciences, Magyar Tudósok körútja 2, H-1117, Budapest, Hungary.

[e] Université d'Angers, MOLTECH-Anjou UMR CNRS 6200, Group Linear Conjugated Systems, 2 Boulevard Lavoisier, 49045 Angers, Franc.e

*Corresponding author:

David Rondeau, Université de Rennes, Institute d'Electronique et de Télécommunications de Rennes IETR UMR CNRS 6164, Campus de Beaulieu, 263 avenue du Général Leclerc, 35042 Rennes Cedex, France. Email: david.rondeau@univ-rennes1.fr

Dedicated to Professor Jean-Claude Tabet on its 75th Birthday and for his contribution to unimolecular chemistry of gaseous organic ions

Abstract

The self-rigidification of ionized π-conjugated systems based on two combinations of thiophene (T) and 3,4-Ethylenedioxythiophene (E) is investigated using mass-analyzed ion kinetic energy spectrometry (MIKES) of ions produced from electron impact ionization at 70 eV. The *m/z* 446 radical cations of the two isomers **ETTE** and **TEET** lead to detect *m/z* 418 and 390 daughter ions. The MIKE spectra differ only by the intensities of these fragment ions. As the *m/z* 418 daughter ion is produced through a same retro-Diels Alder reaction whatever

the fragmenting isomer, the difference in daughter ion intensities is interpreted in term of unimolecular dissociation rate constants ($k(E_{int})$) ratios. Considering that the transition state (TS) of such reaction is attributed to a quinoid form, equivalent vibration modes are assumed for the TS of both dissociating **ETTE** and **TEET** radical cations. As a result, by using the Rice–Ramsperger–Kassel–Marcus (RRKM) theory, the difference in daughter ion intensities is interpreted by considering that the fragmenting ion is more or less ordered in its ground state than at the transition state, resulting from the influence of the number of the S···O interactions in the planarization of the **TEET** ion toward the **ETTE** charged species. The comparison of this behavior in MIKES experiments is supported by the modelling of ion behavior in mass spectrometer and the calibration in internal energy of the radical cations produced in an EI source.

Keywords

Conjugated systems, oligothiophenes, RRKM, MIKES, unimolecular dissociations

Introduction

Owing to a unique combination of moderate band gap, stability and structural versatility, thiophene-based pi-conjugated systems have been a focus of considerable fundamental and technological interest for almost four decades.[1] In this context, the control of the energy levels of frontier orbitals and hence of the band gap of the corresponding materials represent key issues for the potential applications of these materials in organic (opto)electronics and photovoltaics.[2,3] The design and synthesis of low band gap thiophene-based conjugated systems has been developed along different approaches such as the increase of the quinoid character of the thiophene ring, the synthesis of systems containing alternating electron-releasing and electron-withdrawing groups, or the planarization and rigidification of the conjugated backbone by covalent or non-covalent intramolecular interactions.[2] Besides being the monomer of the well-known poly(3,4-ethylendioxythiophene) (PEDOT) initially developed by Bayer.[4] EDOT is also an interesting building block which combines strong electron-donor properties with the ability to planarize and rigidify the π-conjugated systems in which it is inserted by means of intramolecular non-covalent sulfur–oxygen interactions.[5-8]

These phenomena have been investigated in detail on series of hybrid conjugated oligomers based on various combinations of thiophene (**T**) and EDOT (**E**) moieties.[8] An interesting case is given by the comparison of quaterthiophenes **ETTE** and **TEET** (Scheme 1). In fact, whereas **TEET** is fully rigidified by four intramolecular S…O interactions, for **ETTE** only

the two **ET** pairs are rigidified by a single S…O interaction while a free rotation is possible around the central **T-T** single bond (**Scheme 1**).

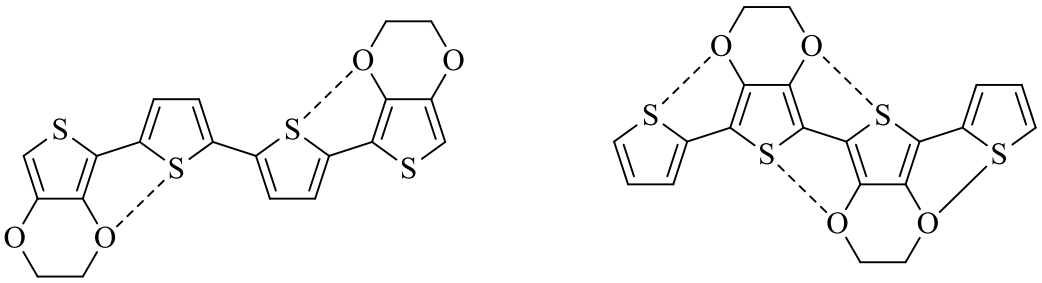

ETTE **TEET**

Scheme 1: Chemical structures of **ETTE** and **TEET** rigidified by non-covalent sulfur-oxygen interactions (dashed lines).

The crystallographic structure of these two compounds has been reported and their electronic properties have been investigated by UV-Vis absorption spectroscopy and cyclic voltammetry. The results provide a coherent picture showing that moving the two **E** units from the outer to the inner positions leads to a more rigid structure as confirmed by X-ray data and by the exaltation of the vibrational fine structure of the absorption spectrum. On the other hand, the CV of the two compounds show that this structural modification leads to a negative shift of the first oxidation potential with a large increase of the difference between the first and second anodic peak potential (from 270 to 440 mV). These results indicate a better electron delocalization in the radical cation in **TEET** but a strong increase of the coulombic repulsion between positive charges in the dication state (**Figure 1**).[8]

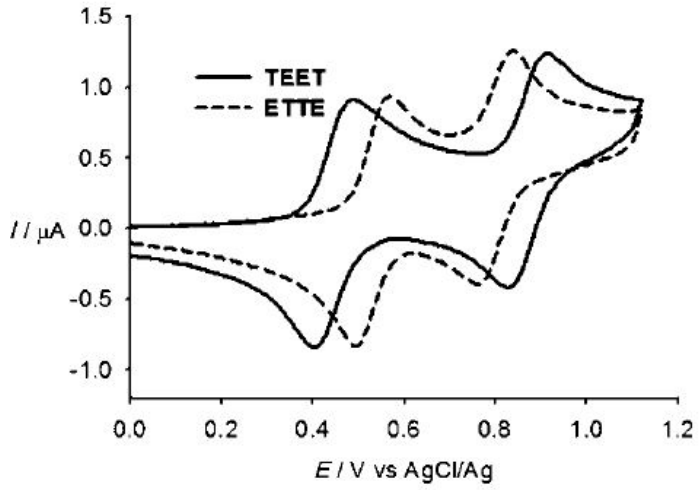

Figure 1. Cyclic voltammograms of **ETTE** and **TEET** in 0.10 M Bu_4NPF_6/DCM, scan rate 100 mV s^{-1} (reprinted with permission from Ref 8).

To summarize, the major role of EDOT in the self-rigidification and planarization of π-conjugated systems is well-established, and namely the influence of its position on the oligomer physico-chemical properties as highlighted by the measurements performed from the **TEET** and **ETTE** isomers.[5-8] However, whereas this behaviour has been widely demonstrated for neutral species, experimental evidences for the occurrence of such effects on radical cations are still lacking.

Mass spectrometry can provide a suitable tool for studying the intrinsic behaviour of such charged species through the ion unimolecular dissociation reactions. The structural identification performed for validating the synthesis of the **ETTE** and **TEET** compounds has previously shown that their low resolution mass spectra recorded using electron impact (EI) ionization, exhibit the same fragment ions *m/z* 418 and *m/z* 390. In these ion source mass spectra, the *m/z* 390 ion intensity is greater than that of the *m/z* 418 in the case of the **ETTE** radical cation fragmentation whereas the opposite result is obtained for **TEET**. In the theory of mass spectra, the ion intensities are related to their dissociation kinetics.[9] As a result, we assume that the difference in ion intensity ratios is a function of the vibration mode of each of the two fragmenting oligomers **ETTE** and **TEET**. The aim of this paper is then to account for the difference in planarization of these π-conjugated systems. For highlighting this property we have simulated the behaviour of these ions that dissociate in the second field free region (FFR2) of a designed magnetic mass spectrometer using the MassKinetics Software.[10]

Theory

In mass spectrometry, the ion decay due to dissociation processes depends on the fragmentation reaction rate ($k^{i,j}(E_{\text{int}})$) of an ion *i* at a given internal energy (E_{int}) producing a fragment ion *j*. The value of $k^{i,j}(E_{\text{int}})$ can be calculated using the RRKM formalism developed in the context of the transition state theory (TST) such as:[11,12]

$$k^{i,j}(E_{\text{int}}) = \frac{\sigma}{h}\frac{N^{\ddagger}\left(E_{\text{int}} - E_0\right)}{\rho(E_{\text{int}})} \qquad (1)$$

where, σ is the reaction degeneracy, *h* is Planck's constant, E_0 is the reaction critical energy, $N^{\ddagger}(E_{\text{int}}\text{-}E_0)$ is the sum-of-states at the transition state (TS) from 0 to $E_{\text{int}}\text{-}E_0$ and $\rho(E_{\text{int}})$ is the density of states of the dissociating ion at an energy level equal to E_{int}. The evaluation of the sum and density of states is usually done by a direct count using the Beyer–Swinehart algorithm with the harmonic oscillator model applied with internal rotations approximated by low-frequency vibrations.[13] The frequency file of an ion in its ground state is usually obtained from quantum chemical calculations. To evaluate the vibration frequency file of the activated complex at the TS, a frequency value close to the vibration mode corresponding to the reaction coordinate (CR) is removed and five other frequencies are scaled to obtain a value of the well-known Arrhenius pre-exponential (A_{pe}) factor.[14] This one is considered as a convenient parameter for describing the differences between the vibrational frequencies of the reacting ion and the TS.[15] The A_{pe} factor is related to the vibrational activation entropy difference ($\Delta_r^{\neq} S_m^{\circ}$).[16,17] An A_{pe} value of the order of 10^{14} characterizes dissociation reactions where few oscillation modes disappear between the reactant ion and the TS.[18] Conversely, ~ 10^{10} A_{pe} values are in agreement with unimolecular dissociation reactions where a fragmenting ion is less ordered at its ground state than at the TS.[18] For an ion taken at a given E_{int} that dissociates via two competitive channels, the relative daughter ion intensities are related to the relative magnitudes of the reaction rate constants $k^{i,j}(E_{\text{int}})$ characterizing the ion dissociation process *j*. In the case of the studied oligomers **ETTE** and **TEET** where *i* is related to the *m/z* 446 parent ion and *j* either to the *m/z* 418 or 390 daughter ion, one can state that the ratios of the rate constants and the daughter ion intensities (I_j) are such that: $\frac{k^{m/z\,446,\,m/z\,390}\left(E_{\text{int}}\right)}{k^{m/z\,446,\,m/z\,418}\left(E_{\text{int}}\right)} \propto \frac{I_{m/z\,390}}{I_{m/z\,418}}$ (2). At a given E_{int}, the fragment ion intensities of the each isomer oligomer are related to the ratios of the dissociation rate constants that roughly depends on the $A_{\text{pe}}(i \rightarrow j)$ factor and the fragmentation critical energy $E_0(i \rightarrow j)$ characterizing

each dissociation processes. Such an assumption is valuable because the deposited energy during the ionization process at 70 eV of the ionizing electron kinetic energy is considered as reproducible for these two isomers that fragment through the same dissociation mechanism.[19] As a result, if $E_0(i \rightarrow j)$ is evaluated from theoretical calculations and by assuming that the TS of the reaction leading to the isobaric ions have the same vibrational properties whatever for the **ETTE** or **TEET** dissociating ion, then the measured differences in term of ion intensities depend only of the relative planarization of the reacting ion at its ground state.

The Mass Kinetics algorithm generates theoretical mass spectra from simulated mass spectrometric processes. It is a general framework that allows for calculating dissociation reaction rates, transition probabilities between different ion states and the abundances of the ions moving through different parts of a mass spectrometer whose geometry and acting parameters are modelised.[10] In MassKinetics the ions are characterized by their internal and kinetic energies that's define the 'state' of a given ion. The MassKinetics modelling was namely applied to the internal energy distribution $P(E_{int})$ evaluation of ions emitted in electrospray ionization sources interfaced with different mass spectrometers,[20-24] ion-molecule reaction studies in the application field of the collision activated reaction experiments (CAR)[25] and kinetic energy release determination (KERD) of metastable ions fragmenting in sector mass spectrometer.[26,27]

For the present work, the ion intensity theoretical ratios (see **equation 2**) have been compared with the measurements performed from Mass-analyzed Ion Kinetic Energy Spectrometry (MIKES) experiments. The considered adjusting parameter was the A_{pe} factor since the E_0 values are inspired from literature data. The calibration in E_{int} of such experiments has been performed by a preliminary study that allows us to evaluate the internal energy distribution $P(E_{int})$ of reacting ions by using the well-known reactivity of the butylbenzene radical cation. The latter is considered as a thermometer ion for calibrating the internal energy deposited in compounds ionized under EI at 70 eV electro, kinetic energy.[28-32]

Materials and Methods

Chemical

The two oligomers have been synthesized by Stille coupling reactions as already described.[8] Thus, ETTE was obtained in 78 % yield by reacting a slight excess of stannic derivative of EDOT onto 5,5'-dibromo-2,2-bithiophene. For TEET, an excess of 2-bromothiophene was coupled to the bisstannic derivative of bis-EDOT leading to the target molecule in 50% yield.

Chemical quantum calculation

All calculations were performed using the Gaussian 09 software package.[i] Optimization of geometries, frequency and single point energy calculations were done using the B3LYP functional[ii] with the basis set 6-31G**[iii]

Table 1.

Species	Frequencies (cm^{-1})
ETTE$^{+\cdot}$	14.7781, 24.2967, 32.451, 51.2292, 54.744, 64.78025, 71.6467, 93.3491, 118.1759, 118.6637, 127.7883, 131.403, 152.9306, 204.2305, 237.3951, 246.5148, 270.1342, 286.4081, 294.705, 302.9554, 326.7571, 331.6722, 337.1649, 359.1209, 377.7158, 408.5628, 432.2587, 442.0483, 445.0325, 463.2977, 466.1725, 491.2019, 525.9638, 534.1049, 539.8441, 563.9237, 571.5896, 575.0289, 600.3725, 619.3317, 623.641, 676.3201, 686.8397, 687.2083, 710.8755, 714.4668, 719.0218, 721.5513, 756.2104, 756.351, 804.1023, 806.2175, 831.8609, 842.7323, 847.0719, 848.7099, 851.4357, 863.1136, 893.2099, 923.6775, 924.0408, 924.4677, 925.4211, 974.3411, 975.1957, 1034.789, 1034.997, 1081.277, 1082.4781, 1111.2368, 1121.9258, 1121.9502, 1129.2378, 1187.9126, 1187.9435, 1200.4771, 1217.6511, 1218.1506, 1229.628, 1249.5906, 1257.8399, 1270.7136, 1271.9574, 1299.9722, 1300.2818, 1341.2872, 1356.8101, 1393.2175, 1398.3628, 1406.3583, 1407.9944, 1424.9165, 1453.0954, 1486.8311, 1491.9274, 1497.9765, 1501.1987, 1503.1348, 1509.1699, 1509.3635, 1515.6512, 1535.5828, 1539.3897, 1562.7833, 1602.7584, 1604.2338, 3055.8308, 3055.9153, 3075.5945, 3075.6835, 3148.6834, 3148.747, 3156.1031, 3156.1836, 3224.3984, 3224.5757, 3238.822, 3239.0116, 3277.1731, 3277.2708.
TEET$^{+\cdot}$	17.7456, 32.5934, 41.1536, 46.6115, 48.0676, 62.0258, 88.4792, 93.8283, 115.3735, 121.1345, 123.8487, 126.6391, 160.406, 173.962, 182.31, 187.3394, 276.692, 279.5059, 290.0405, 293.5251, 310.9618, 317.0324, 333.7848, 367.3828, 375.4123, 416.1914, 437.9046, 443.6289, 454.5716, 463.3623, 473.2906, 493.2066, 532.468, 551.0293, 557.6897, 565.4454, 570.1607, 580.7569, 591.1948, 608.0718, 632.8551, 634.7961, 663.8649, 666.9149, 726.9724, 732.1068, 732.2611, 734.4542, 735.5444, 807.3867, 836.9753,

	841.2386, 841.2467, 842.3874, 849.7377, 858.0485, 868.7851, 877.8653, 880.2008, 933.5599, 933.5636, 940.5003, 970.5445, 971.0538, 1004.0621, 1013.9462, 1034.1009, 1091.5824, 1099.3335, 1101.1696, 1112.1386, 1112.8516, 1119.9765, 1120.4341, 1125.804, 1159.5993, 1182.1755, 1242.0361, 1245.2093, 1266.2994, 1266.5342, 1294.6453, 1298.3694, 1299.8216, 1306.6013, 1341.6400, 1377.2657, 1377.4752, 1392.8866, 1406.3032, 1410.5102, 1434.3349, 1441.5604, 1461.1253, 1467.1583, 1496.9829, 1497.5518, 1504.8061, 1506.426, 1511.6195, 1528.9704, 1533.6523, 1533.7089, 1566.779, 1572.9027, 1580.3773, 3065.9801, 3066.1097, 3077.0721, 3077.1391, 3155.0965, 3155.1227, 3158.5929, 3158.6123, 3222.3574, 3222.3912, 3242.8572, 3242.9021, 3266.842, 3266.8664

Table 1: Frequency file obtained from theoretical

Mass Spectrometry

Experiments were performed on a JMS-700 double-focusing (B/E) mass spectrometer with reversed geometry (JEOL, Akishima, Tokyo, Japan). The analytes were introduced in the ion source *via* a direct inlet probe equipped with a cooling water device that keeps the sample temperature at a constant value. Calibration compound (PFK) was introduced into the mass spectrometer ion source via the standard sample inlet device. Ions are produced by Electronic Impact (EI) ionization in positive ion mode with a 300 μA ionizing current and a 70 eV ionizing energy. Depending on the experiment, the source temperature was kept at 200 °C or 300 °C. Low-resolution full-scan mass spectra (typically R = 1000 at 10% valley) were obtained by scanning the magnetic field over a wide range of mass-to-charge ratios while keeping constant the electric field for an accelerating voltage (V_{acc}) value of 10 kV. Elemental composition of the ions was checked by high resolution measurements (typically R = 10000 at 10% valley) using an electric field scan method with PFK ions as internal standard. In this case, the accelerating voltage (V_{acc}) and the electric field are scanned while the magnetic field is being kept constant. Metastable ion (MI) spectra were obtained by the MIKES experiments where the dissociations take place in the second field-free region (FFR2), *i.e.* after the magnetic sector and before the electric sector. The molecular ion ($M^{+\cdot}$) produced from analysed compounds, was selected using the magnetic sector and the product ions were analysed by scanning the electric filed while the magnetic field is kept constant for a V_{acc} value fixed at 10 kV. For the measurement of the survival yields (SY) and the ratios of the daughter ion amounts, the MIKE spectra were collected by averaging the signals measured on

each set of ten MIKE scans. Each MIKE spectrum was treated by the SigmaPlot™ Software in order to express the number of ions *via* the calculion of the area under the detected peak. Note that for all the measurements related to the metastable ion formation, the voltage values of the different part of the ionization chamber were maintained at constant values, *i.e.* the voltage of the ion accelerating refinement, the repeller lens, the first and the second focus lenses and the deflector lens. The determination of ion survival yields (*SY*) was performed using the well-known equation (3) such as: $SY = \frac{I_{P^+}}{I_{P^+} + \sum_{i=1}^{n} F_i^+}$ (3), where in the case of the butylbenzene full scan mass spectra, I_{P^+} is the intensity of the *m/z* 134 parent ion, and $\sum_{i=1}^{n} F_i^+$ is the sum of the two fragment ions at *m/z* 92 and 91.

Mass spectra modelling

Theoretical survival yields and ion abundance ratios were calculated using the MassKinetics software (ver. 1.17), available at http://proteomics.ttk.mta.hu/masskinetics/. The simulations performed by MassKinetics use internal and kinetic energy distribution functions together with the probabilities that describe transition between different states of an ion. For the present study, the considered changes in kinetic and internal energies of the ions in the gas phase are due to acceleration in electromagnetic fields and energy partitioning in chemical reactions.

In the case of the butylbenzene ion fragmentation, the $\rho(E_{int})$ and $N^{\ddagger}(E_{int}\text{-}E_0)$ (see equation 1) have been evaluated from the frequency models of the ground and the transition states proposed by Muntean and Armentrout ; the σ and E_0 values of the *m/z* 134 → *m/z* 91 and *m/z* 134 → *m/z* 92 reactions are also considered from the same paper.[32] In the case of the **TEET** and **ETTE** radical ions the values of σ and E_0 will be further indicated in the text (*vide infra*). For evaluating the $\rho(E_{int})$ term of theses radical cations in their ground state, the vibrational frequency values were obtained from theoretical calculations at a B3LYP/6-31+G** level of theory (*vide supra*). For evaluating the TS frequency file of the *m/z* 446→ *m/z* 418 and *m/z* 446→ *m/z* 390 reactions, a frequency of value typically close to 1200 cm^{-1} is removed and five other frequencies are scaled to obtain the expected A_{pe} value. It must be mentioned that in this frequency range encompassing the 1000 to 3000 cm^{-1} value, the influence of the magnitude of the removed vibration on the RRKM calculation results can be considered as

very low. The Mean Thermal Energies at 473 K ($\langle E_{\mathrm{Therm}}(473\,\mathrm{K})\rangle$) of the **ETTE** and **TEET** radical cations that correspond to the source temperature can be calculated from the frequency files of the **Table 1** by using the **Equation 4** such as:

$$\langle E_{\mathrm{Therm}}(473\,\mathrm{K})\rangle = \sum_{i=1}^{s} \frac{h\nu_i}{e^{\left(h\nu_i / k_B T\right)} - 1} \quad (4)$$

In equation 4, k_B is Boltzmann's constant, T is the temperature and v_i is the frequency value of a vibration mode i considered among the s oscillators of the radical cation. From this $\langle E_{\mathrm{Therm}}(473\,\mathrm{K})\rangle$is of 1.392 eV and 1.396 eV for **ETTE**$^{+\cdot}$ and **TEET**$^{+\cdot}$, respectively. This two close values indicate that the frequency levels of these two radical cations at their ground state, do not account *a priori* for the relative rigidifications of so-called S…O interactions. This is thus rather the magnitudes of $A_{\mathrm{pe}}(i \rightarrow j)$ that will evidence the relative planarization of the **ETTE** and **TEET** ions at their ground state. Two mass spectrometer geometries have been modelised for accounting for the mass spectrometric experiments with MassKinetics. For the full scan mass spectrometry experiments the following sequence was used: (1) gaseous molecule initially considered with thermal internal and kinetic energy distributions evaluated either at 473 K or at 573 K; (2) a Gaussian deposited energy function considered to account for the energy transfer during the ionization process; (3) acceleration under a 10 kV potential difference (flight length: 1.6 cm); (4) ion selection followed by detection (field-free flight from the source to the detector with 1.9656 m flight length). For a MIKES experiment, the following events have been built up as followed: (1) to (3) are identical as described above; (4) field-free flight (from the acceleration lens to the beginning of the FFR2 with a 0.966 m flight length); (5) Ion selection (*m/z* 446); (6) field-free flight (through the FFR2 with a 0.449 m flight length); (7) ion selection by scanning the electric analyser followed by detection (field-free flight from the end of the FFR2 to the detector with 0.55 m flight length).

Results and discussion

Calibration in internal energy of ions produced in the EI source experiments

The ratios of the intensities of the *m/z* 91 and 92 fragment ions produced from the two competitive reactions of the butylbenzene molecular ion and the survival yield of the *m/z* 134 parent ion, have been calculated by the MassKinetics software and compared to the experimental values measured from the EI mass spectra (see **Table 2**). The fitting parameter

between experiment and simulation is the initial internal energy distribution of the ionized compounds. This distribution associates two components. One of them is the thermal energy of the molecule (P(E_{Therm})) vaporized in the EI source under a 473 K or a 573 K temperature and the other takes into account the deposited energy during the ionization process (P($E_{\text{Ionization}}$)). The latter is a Gaussian like distribution that does not depend of the source temperature. The thermal component is based on the ergodicity principle assuming that the thermally excited states of all the vibrational modes can be reached with the same probability leading to the expression: $P(E_{\text{Therm}}) = \frac{\rho(E_{\text{int}}) \cdot \exp\left(-E_{\text{int}} / k_B T\right)}{\int_0^{\infty} \rho(E_{\text{int}}) \cdot \exp\left(-E_{\text{int}} / k_B T\right)}$ (5). The internal energy deposited during the interaction of a gaseous molecule with an electron beam at a 70 eV kinetic energy can be expressed from a Gaussian like function such as: $P(E_{\text{Ionization}}) = \frac{1}{w\sqrt{\pi/2}} e^{-\frac{1}{2}\left(\frac{E - X_c}{w}\right)^2}$ (6), where w and X_c are the so-called width and position terms, respectively. The initial internal energy distribution (P(E_{int})) of a butylbenzene radical cation is the result of the contribution of the two distributions $P(E_{\text{Therm}})$ and $P(E_{\text{Ionization}})$. In this study, the best fit between experiment and theory (see **Table 2**) has been obtained for T = 473 K (see **Equation 5**) and w = 5.5 eV and X_c = 3.5 eV (see **Equation 6**). The contribution of these two components in the total internal energy distribution (P(E_{int})) is illustrated in **Figure 2**. This initial internal energy distribution (P(E_{int})) was considered for the rest of the study as a calibration in internal energy of the ionization source.

	Experimental Data		Theoretical data	
Source temperature	473 K	573 K	473 K	573 K
$I(m/z\,91) / I(m/z\,92)$	1.72	2.06	1.77	1.94
Survival Yield	0.16	0.14	0.13	0.10

Table 2: Measured and simulated data related to intensity ratios of fragment ions and SY values of the butylbenzene radical cation obtained from experimental and theoretical EI full scan mass spectra.

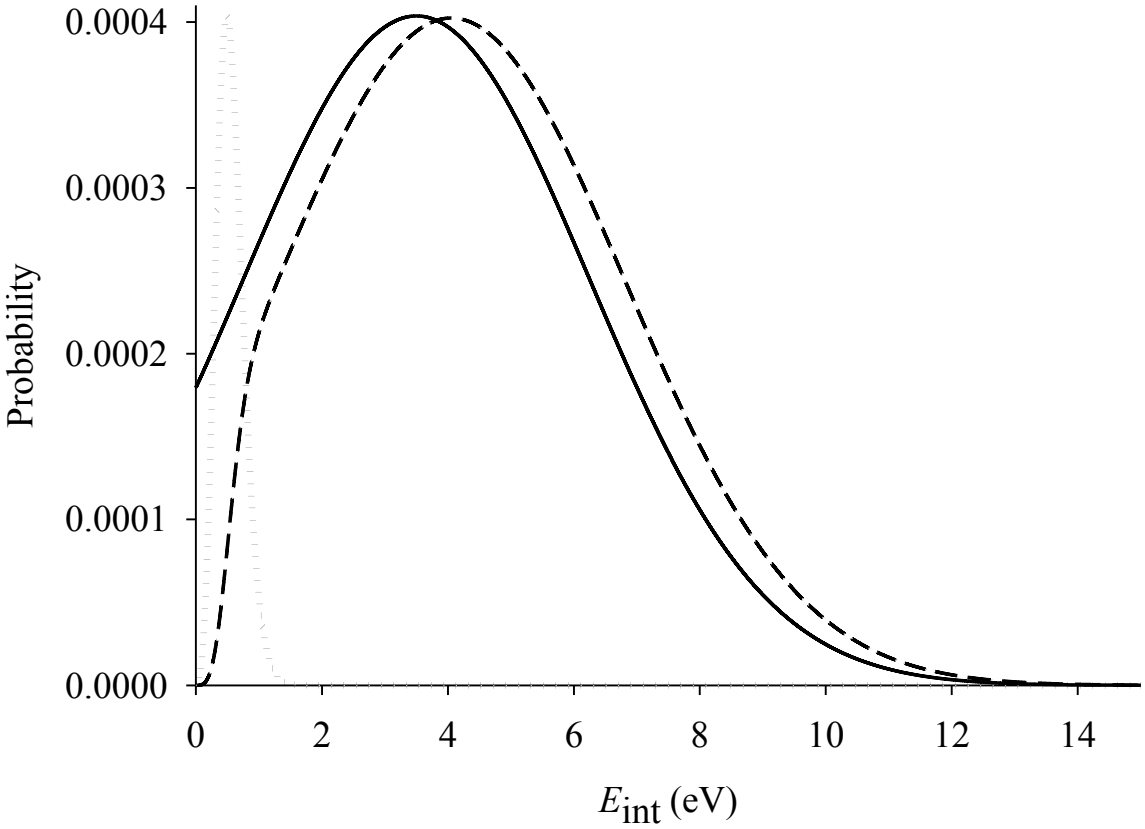

Figure 2: Contribution of the thermal (P(E_{Therm})) (dotted line) and ionization energy distribution (P($E_{Ionization}$)) (solid line) to the initial distribution of the butyl benzene molecular ion produced in the EI source of the JMS 700 sector mass spectrometer (dashed line). Note that for a better reading of the figure, the maximum of the P(E_{Therm}) curve has been equalized with that of the P($E_{Ionization}$) distribution.

The internal energy distribution of the *m/z* 134 ion population changes as a function of it position into the mass spectrometer analyzer. At the entrance of the second field free region (FFR2), this distribution will depend of the own reactivity of the butylbenzene molecular ion. Even though the internal energy distribution of the *m/z* 134 ions can be calculated as their reach the FFR2, this one cannot be actually considered for calibrating EI-MIKE experiments performed from other ionized compounds. The later have indeed their own unimolecular reactivity under electron impact and their $P(E_{int})$ in FFR2 will depend of this reactivity in the source itself and into the analyzer before reaching this zone. As a result, the best way for calibrating the EI-MIKE experiments is to consider the butylbenzene radical cation as a thermometer ion only for calibrating the internal deposited during the ionization process and thus to apply this calibration to any ionized compound. This procedure can be considered all

the more that it can be used to calibrate internal energy of the EI-MIKE spectra for that a fragmentation that occurs in the second field free region of the mass spectrometer. In our case, a ratio between the intensities of the *m/z* 91 and 92 has been evaluated as being greatly favorable to the formation of the later in agreement with that was documented.[14]

Behavior of π-conjugated oligomers containing 3,4-ethylenedioxythiophene (EDOT) in EI-MIKES experiments

Typical EI-MIKE spectra recorded from the selection of the *m/z* 446 ion of the radical cation ($M^{+\cdot}$) of the **ETTE** and **TEET** compounds are depicted in **Figure 3a** and **3b**, respectively.

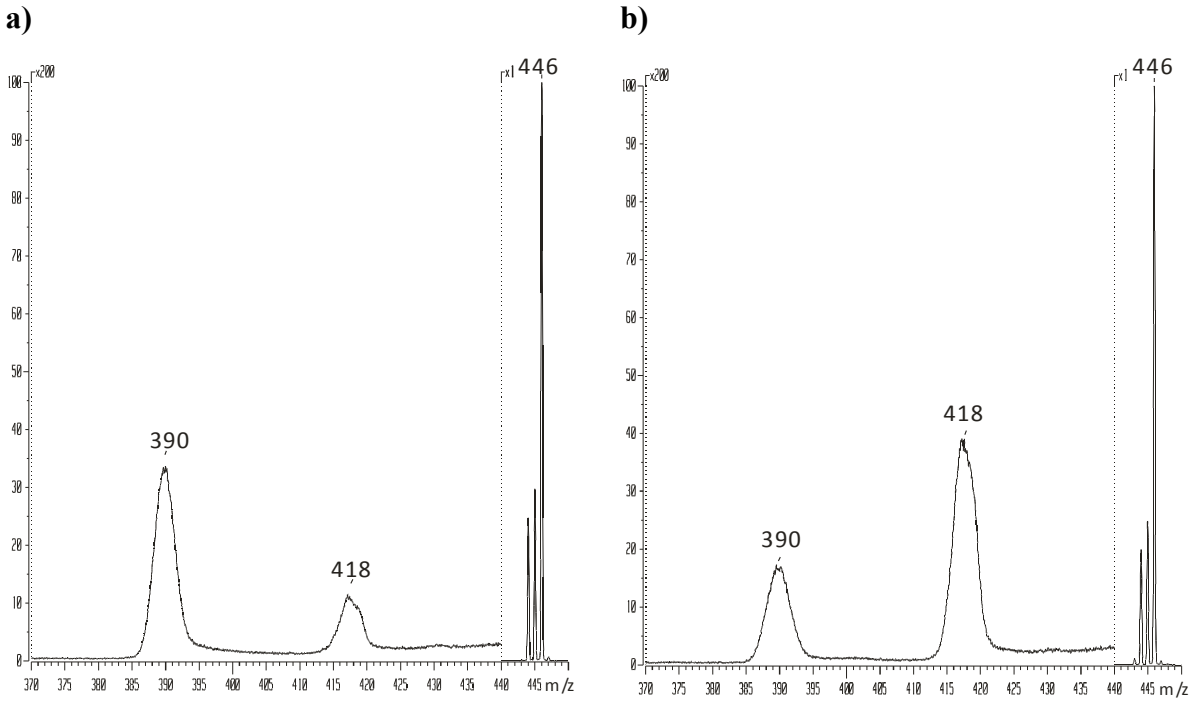

Figure 3: MIKE spectra of the molecular ion (*m/z* 446) of the **ETTE** (**a**) and **TEET** (**b**) compounds.

Figure 3 shows that the ratios between the intensities of the *m/z* 418 and 390 fragment ions yielded from metastable decompositions are reversed as a function of the fragmenting ion. The experimental values of the $\frac{I_{m/z\,390}}{I_{m/z\,418}}$ ratios are indeed of 3.80 and 0.55 for the dissociation of the **ETTE** and **TEET** radical cations, respectively. For each compound, the elemental composition of the molecular ion and the *m/z* 390 and 418 fragment ions had been checked from high resolution full scan mass spectra. The comparison between calculated and measured mass are regrouped in **Table 3**.

Compound	Assigned Ion	Measured Mass (u)	Elemental composition	Theoretical Mass (u)
ETTE	$M^{+\cdot}$	445.9781	$C_{20}H_{14}O_4S_4$	445.9769
	$[M-C_2H_4]^{+\cdot}$	417.9463	$C_{18}H_{10}O_4S_4$	417.9456
	$[M-C_3H_4O]^{+\cdot}$	389.9509	$C_{17}H_{10}O_3S_4$	389.9507
TEET	$M^{+\cdot}$	445.9783	$C_{20}H_{14}O_4S_4$	445.9769
	$[M-C_2H_4]^{+\cdot}$	417.9464	$C_{18}H_{10}O_4S_4$	417.9456
	$[M-C_3H_4O]^{+\cdot}$	389.9515	$C_{17}H_{10}O_3S_4$	389.9507

Table 3: Results of Exact Mass Measurements Performed from High Resolution Full Scan Mass Spectra of **ETTE** and **TEET** compounds ionized under electronic impact (EI).

The low-resolution full scan mass spectra recorded for the two studied compounds at several low electron kinetic energies (namely at 12 and 15 eV), have indicated roughly the same appearance potentials for the *m/z* 390 than for the *m/z* 418 ion for the **TEET** and **ETTE** radical cations. This behaviour is in agreement with metastable decompositions that are due to competitive unimolecular reactions rather than consecutive dissociations. From these data and the results of the literature, the fragmentation reactions of the *m/z* 446 molecular ion of the **ETTE** and the **TEET** compounds yielding the *m/z* 418 and 390 daughter ions, can be described as reported in **Schemes 2** and **3**, respectively. The relative formation enthalpies of the structures **1a-1c** and **2a-2c** are regrouped in **Table 4** for the two studied series **ETTE** and **TEET**.

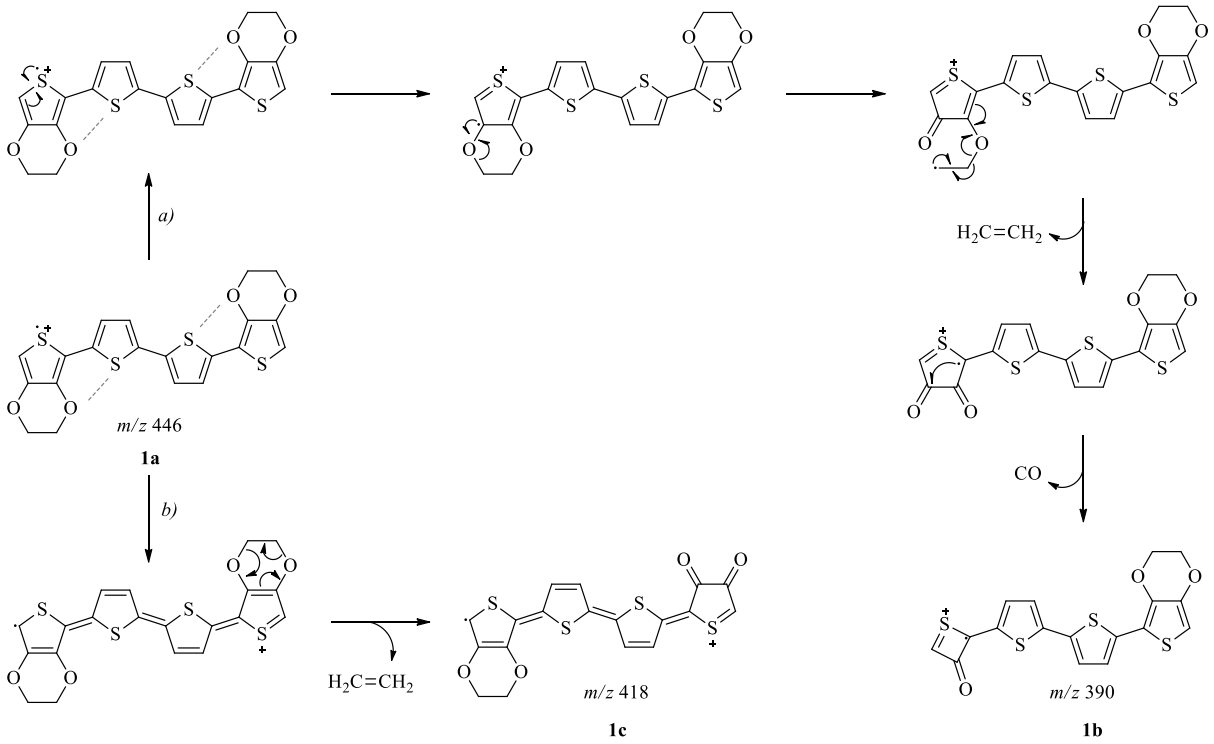

Scheme 2: Proposed dissociation mechanisms of the **ETTE** radical cation (*m/z* 446) to account for competitive metastable decompositions involving either a direct cleavage sequence (pathway *a*) or a retro-Diels Alder process (pathway *b*)

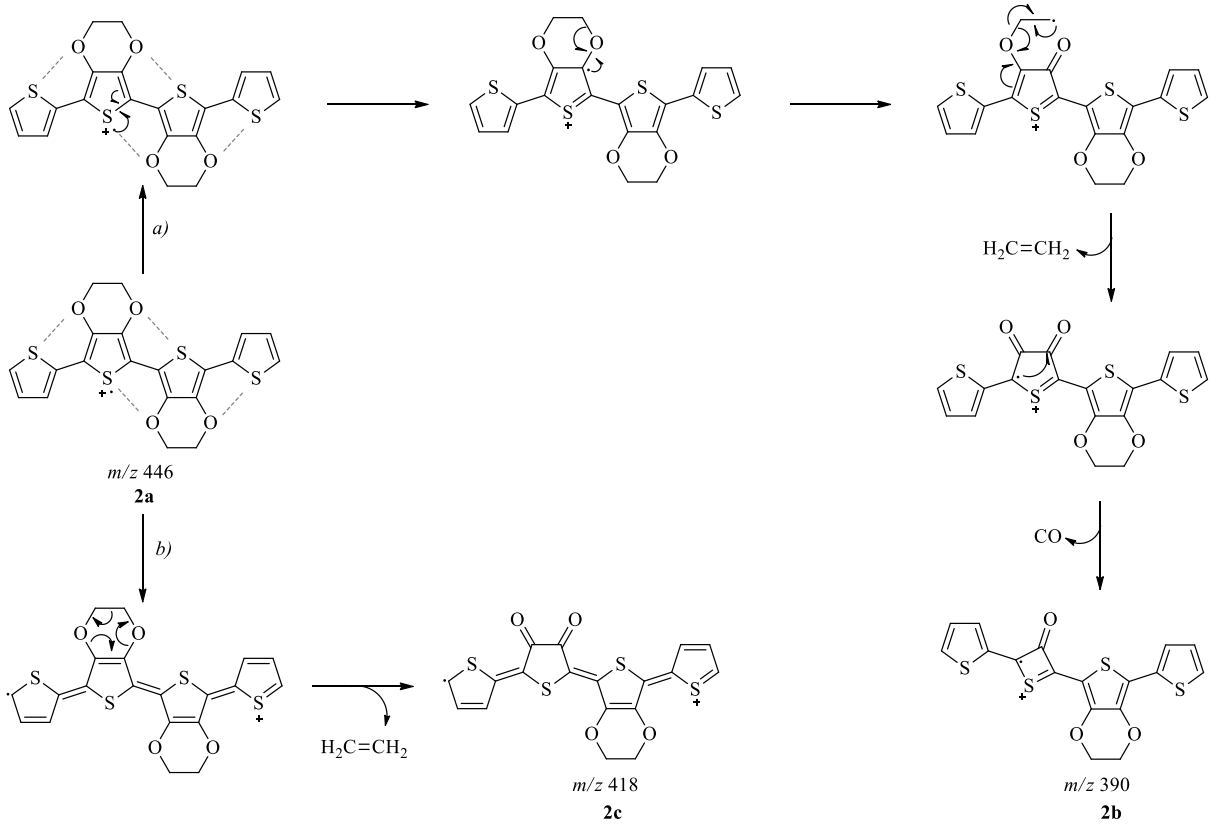

Scheme 3: Proposed dissociation mechanisms of the **TEET** radical cation (*m/z* 446) to account for competitive metastable decompositions involving either a direct cleavage sequence (pathway *a*) or a retro-Diels Alder process (pathway *b*)

Table 4: Becke3LYP/6-31G**Energetics of the dissociation pathways *a)* and *b)* depicted in **Schemes 2** and **3** for the fragmentation reactions of the **ETTE** (**1a**) and **TEET** (**2a**) radical cations.

Structure	Absolutes energies (E)[a]	State	Relatives enthalpy ($\Delta\Delta H_f$) [b]
Ethen (C_2H_4)	-78.542683		
Carbon monoxide (CO)	-113.304423		
1a	-2663.638555	**1a**	0
1b	-2471.697421	**1b** + C_2H_4 + CO	2.56[c]
1c	-2585.030935	**1c** + CO	1.77[c]
2a	-2663.643976	**2a**	0
2b	-2585.048	**2b** + C_2H_4 + CO	2.08[d]
2c	-2471.720478	**2c** + CO	1.45[d]

[a] E values in hartrees including corrections for zero point vibrational energy. [b] $\Delta\Delta H_f$ values in eV considering thermal corrections at 298 K. [c] values in eV relative to ΔH_f(**1a**). [d] values in eV relative to ΔH_f(**2a**).

The dissociation pathways *b*) depicted in the **Schemes 2** or **3** describe a retro-Diels Alder (RDA) mechanism for the *m/z* 446 → *m/z* 418 transition (with reaction degeneracy σ = 2).[33,34] The quinoid form of the structure **1c** and **2c** related to the *m/z* 418 ions produced from the dissociations of **ETTE** (see **Scheme 2**) and **TEET** (see **Scheme 3**), respectively, suggests that these daughter ions can be characterized by roughly the same vibration modes. In this context, the S…O interactions are not at the origin of the planarization of such a quinoid form. The endothermic reactions observed in mass spectrometry involve an activated complex at the TS characterized by a structure closer to the products than the reactant. The vibration modes in the TS are close to that of the *m/z* 418 daughter ion. This leads to consider a very influence of the S…O interactions on the rigidification of the activated complex at the TS in

the case of a RDA process. This is then the vibration modes of the *m/z* 446 parent ion that will govern in a large extend the magnitude of the rate constant for this fragmentation reaction underwent by the **ETTE** and **TEET** radical cations. Considering the dissociating ion at its ground state, the vibration frequency values and namely those that are characteristics of the internal rotations along the central bond of **ETTE** or **TEET**, will be influenced by the self-rigidification of the system in its non-quinoid form, and thus by the number of S…O interactions (see the dashed grey lines in **Schemes 2** and **3**), *i.e*. two and four for **ETTE** and **TEET**, respectively. A defined TS can be associated to the dissociation pathways *b)* (with σ = 2) (see **Schemes 2** and **3)** in agreement with the mechanisms proposed for such a RDA process suggesting then to consider a reverse reaction energy for this fragmentation.[33,34] The E_0(*m/z* 446 → *m/z* 418) values are then greater than that calculated from the $\Delta\Delta H_f$ values of the so-called states "**1c** + CO" and "**2c** + CO" in **Table 4**. This reverse critical energy has thus been considered in this work (*vide infra*).

For the formation of the *m/z* 390 daughter ion, the dissociation pathways *a)* (with σ = 4) (see **Schemes 2** and **3)**, describe series of direct bond cleavages. One can postulate that the overall process can be kinetically characterized by a Log(A_{pe}) value close to 14. The lack of well-defined structures at the TS's indicated by this value, leads to consider the $\Delta\Delta H_f$ values of the so-called states "**1b** + C_2H_4 + CO" and "**2b** + C_2H_4 + CO" (see **Table 4**) as the reaction critical energies E_0(*m/z* 446 → *m/z* 390) for **ETTE** and **TEET** transitions, respectively.

In agreement with that has been stated above through the **Equation 2**, the values of the $\frac{I_{m/z\,390}}{I_{m/z\,418}}$ ratios have been calculated using MassKinetics for different A_{pe}(*m/z* 446 → *m/z* 418) values. In this calculation, the values of E_0(*m/z* 446 → *m/z* 390) mentioned above, have been taken into account for the **ETTE** and **TEET** ions with A_{pe}(*m/z* 446 → *m/z* 390) = 10^{14}. For the values of E_0(*m/z* 446 → *m/z* 418), five reverse critical energy values have been considered from 0.2 to 1 eV. The results of this simulation are reported in **Figures 4** and **5** for the reactivity of the **ETTE** and **TEET** radical cations, respectively.

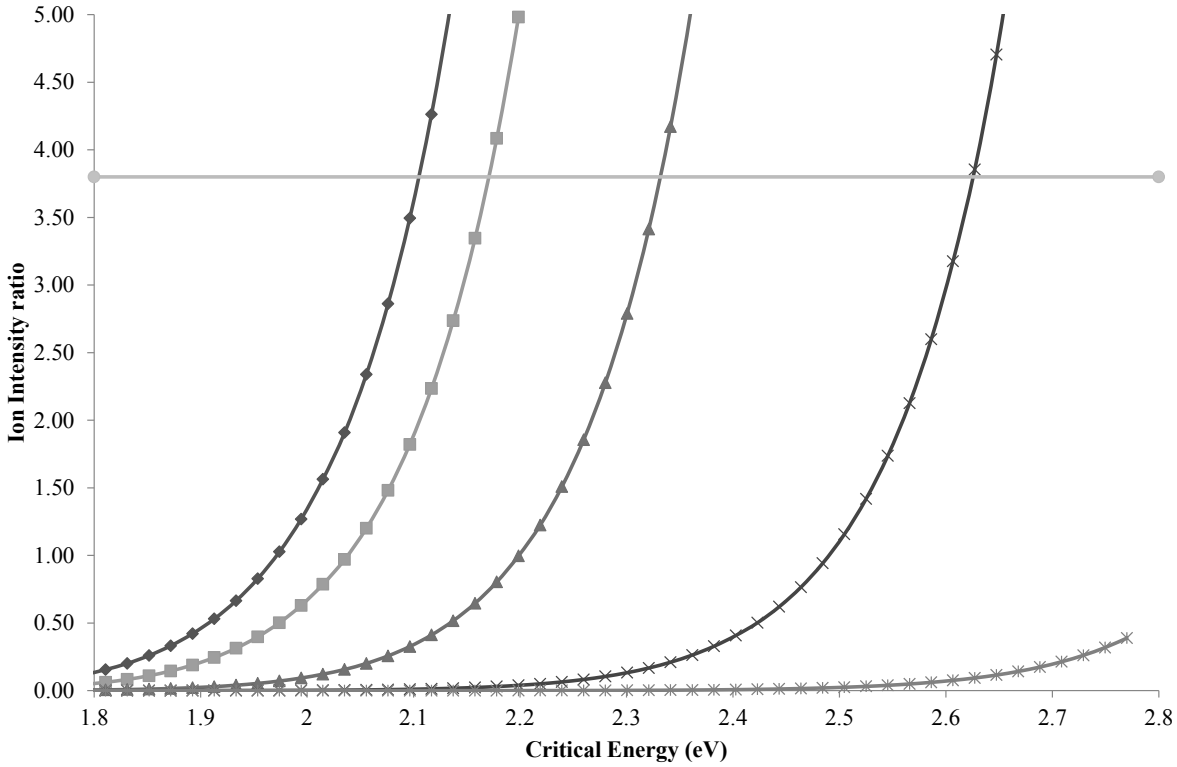

Figure 4: Ion intensity ratios ($I_{(m/z\ 390)}/I_{(m/z\ 418)}$) calculated by the MassKinetics software in an simulated EI-MIKES experiments modelling the dissociation pathways of the **ETTE** radical cation (see **Scheme 2**). The data are plotted as a function of the critical energy E_0(*m/z* 446 → *m/z* 418) for different A_{pe}(*m/z* 446 → *m/z* 418) values of the RDA process (◆: 10^8, ■: 10^{10}, ▲:10^{12} and ×:10^{14} sec^{-1}). Note that in this simulation E_0(*m/z* 446 → *m/z* 390) = 2.56 eV (see **Table 4)** and A_{pe}(*m/z* 446 → *m/z* 390) = 10^{14} (see text). The grey horizontal straight line plotted in the Figure indicates the value of the experimental ion intensity ratio.

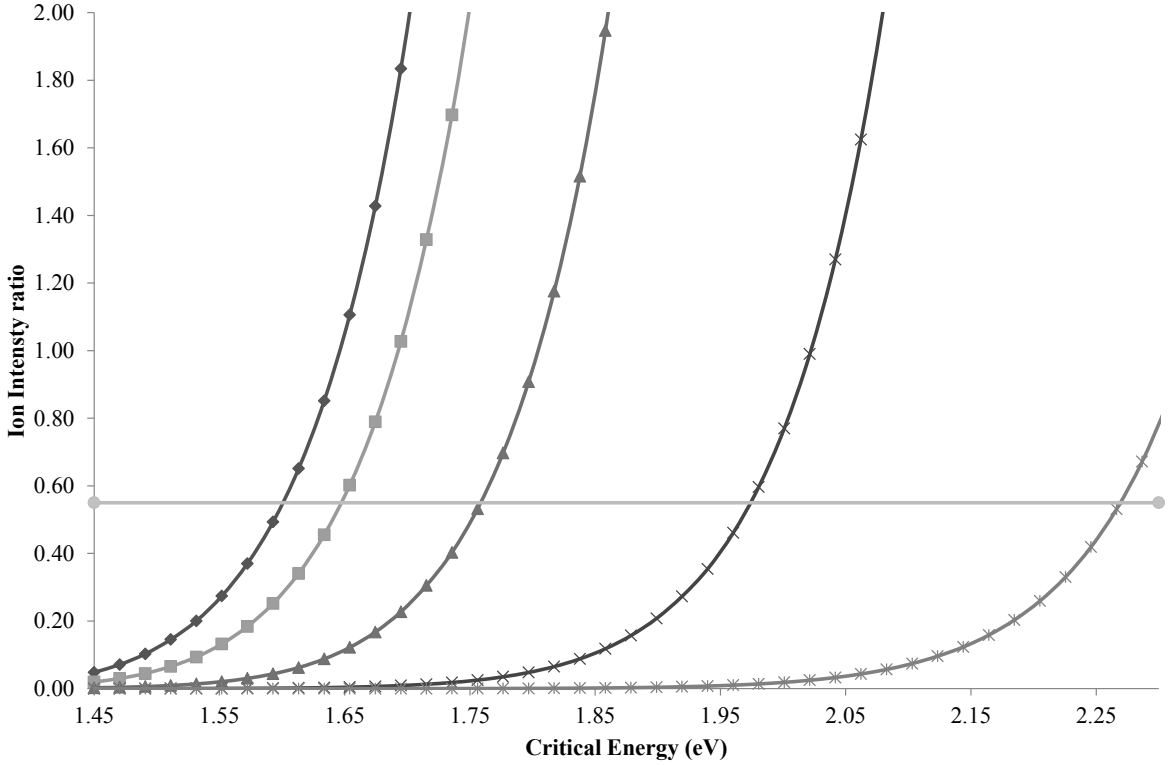

Figure 5: Ion intensity ratios ($I_{(m/z\ 390)}/I_{(m/z\ 418)}$) calculated by the MassKinetics software in an simulated EI-MIKES experiments modelling the dissociation pathways of the **TEET** radical cation (see **Scheme 3**). The data are plotted as a function of the critical energy E_0(*m/z* 446 → *m/z* 418) for different A_{pe}(*m/z* 446 → *m/z* 418) values of the RDA (◆: 10^8, ■: 10^{10}, ▲:10^{12} and ×:10^{14} sec^{-1}). Note that in this simulation E_0(*m/z* 446 → *m/z* 390) = 2.08 eV (see **Table 4)** and A_{pe}(*m/z* 446 → *m/z* 390) = 10^{14} (see text). The grey horizontal straight line plotted in the Figure indicates the value of the experimental ion intensity ratio.

The two curves of the **Figure 4** that describe the evolution of the ion intensity ratios from the *m/z* 446 → *m/z* 418 transition with Log(*A*pe) = 14 and 16, are not representatives of a RDA process. Such values are rather equivalent to that of the direct cleavage characterizing the *m/z* 446 → *m/z* 390 transition. In addition, these curves are plotted form E_0 values that exceed 2.6 eV in magnitude for a reaction occurring via a RDA mechanism. This is not in agreement with literature data suggesting that the critical energy of such reaction should not be greater than about 2 eV.[33,34] Despite this, if one considers that reverse critical energies of a RDA reaction of about 0.3 to 0.5 eV, then the 1.77 eV value of energy level defined by the structure **1b** and the CO molecule (see **Table 4**) will be increased from 2.07 to 2.27 eV. Even though this E_0(*m/z* 446 → *m/z* 418) values exceeds 2 eV, the orders of magnitude of 10^{10} and 10^{12} for the A_{pe}(*m/z* 446 → *m/z* 418) parameter are better in agreement with the experimental data

describing the **ETTE** radical cation behavior. By focusing on the **TEET** radical cation fragmentation, one can state that the same range of reverse critical energy values increase the E_0(*m/z* 446 → *m/z* 418) value for from 1.45 eV (see **Table 4**) to 1.75 and 2.25 eV. In this case, the Figure 5 shows that the best fit between the modeling and the experiment is obtained with A_{pe}(*m/z* 446 → *m/z* 418) values ranging from 10^{12} to 10^{16}. By proposing that a 0.4 eV reverse critical energy leading to E_0(*m/z* 446 → *m/z* 418) values of 2.17 and 1.85 eV for the **ETTE** and **TEET** radical cations, respectively, a refinement of the fit between calculation and experiment allows to propose the Log(A_{pe}) values reported in **Table 5**.

	m/z 446 → *m/z* 390		*m/z* 446 → *m/z* 418		$I_{(m/z\ 390)}/I_{(m/z\ 418)}$
	E_0 (eV)	Log(A_{pe})	E_0 (eV)	Log(A_{pe})	
ETTE$^{+\cdot}$	2.56	14	2.17	9.9	3.93
TEET$^{+\cdot}$	2.08	14	1.85	13	0.53

Table 5: Molecular parameters of metastable dissociations of the two oligothiophenes containing EDOT groups leading to adjust the values of the ratio $I_{(m/z\ 390)}/I_{(m/z\ 418)}$ calculated by MassKinetics (see the last column in the Table) with the data obtained from the MIKES experiments (see **Figure 2**)

The data regrouped in **Table 5** show that A_{pe}(*m/z* 446 → *m/z* 418) for the fragmentation of **ETTE**$^{+\cdot}$ is greatly lower than that of the **TEET**$^{+\cdot}$ dissociation in the case of the RDA process. By referring to the mechanism of the retro-Diels Alder reaction depicted in **Schemes 2** and **3**, the dissociation pathway *b*) involves a quinoid structure of the activated complex at the TS whose self-rigidification is not related to the S…O interactions. This suggests roughly similar values of the sum of state of the activated complex in **Equation 1**. The difference in A_{pe}(*m/z* 446 → *m/z* 418) values is then due to the vibronic structure of the ground state of the dissociating **ETTE** and **TEET** radical cations. The molecular structures depicted in **Scheme 4**, show that for **ETTE**$^{+\cdot}$ the S···O interactions do not prevent the possibility of internal rotation around the central bond (see the rotating arrow in **Scheme 4**), whereas its activated complex (noted as [ETTE$^{+\cdot}$]‡) is getting closer to a quinoid form that is more ordered in term of ro-vibration modes than its ground state. By contrast, in the case of **TEET**$^{+\cdot}$, the dashed grey lines depicted in the **Scheme 4** that illustrate the four S···O interactions in the ground state accounting for a self-rigidification of the system. If one considers the same ro-vibronic structures of the two quinoid forms in each TS of the dissociating ions (noted [ETTE$^{+\cdot}$]$^{\neq}$ and

$[TEET^{+\cdot}]^{\neq}$ in **Scheme 4**), then such a behavior is in agreement with a higher value of A_{pe}(*m/z* 446 → *m/z* 418) for the RDA process underwent by the **TEET** radical cation by comparison to that of **ETTE**.

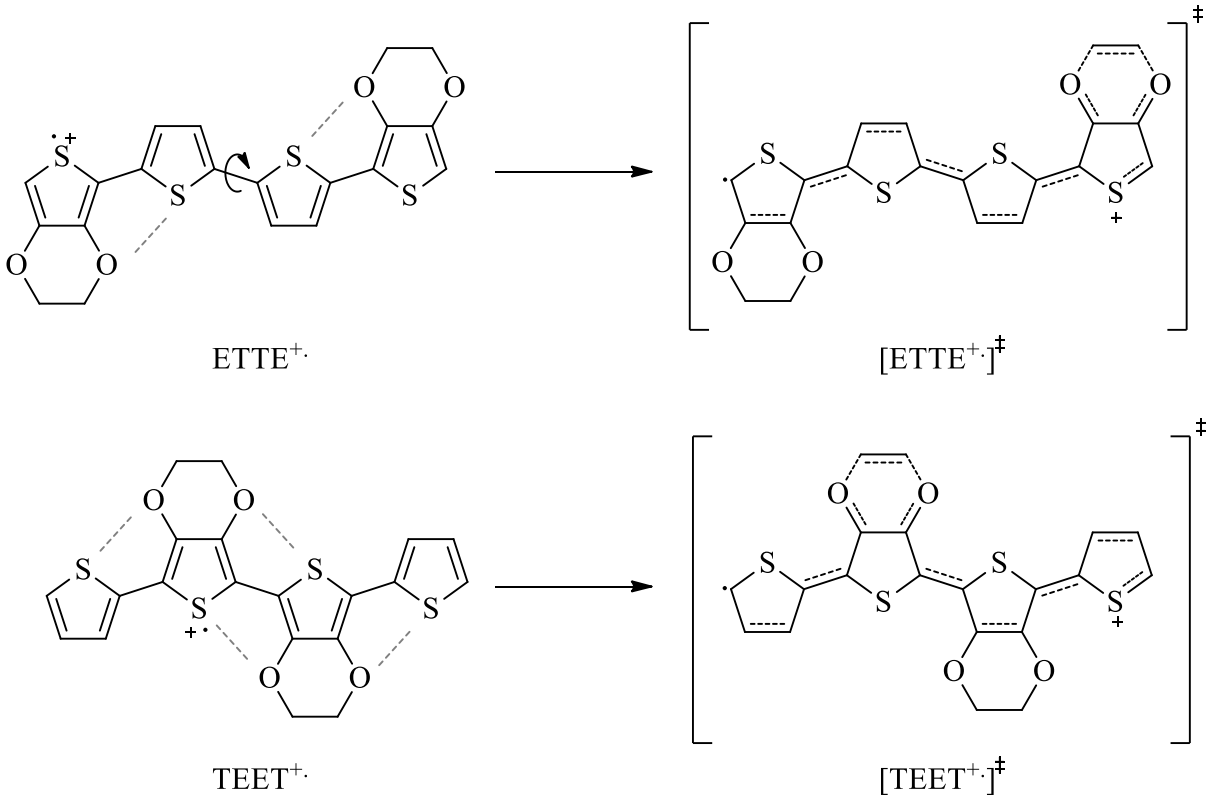

Scheme 4: Illustration of the influence of the S…O interactions in the relative rigidifications of the **ETTE** and **TEET** radical cations at their ground state towards their transition state

Conclusion

This study highlights the fact that experiments as simple to perform than an MIKE spectroscopy, can be able to evidence intrinsic properties of ionized π-conjugated systems by combining them with chemical quantum calculations and mass spectrometry modelling. To our knowledge, this is the first experimental evidence of the influence of the number of the S···O interactions in the planarization of the π-conjugated oligomers containing 3,4-ethylenedioxythiophene at their ionized state.

References

1. Roncali J. Conjugated poly(thiophenes): synthesis, functionalization, and applications. *Chem. Rev.* 1992; 92: 711.

2. Roncali J. Molecular Engineering of the Band Gap of π-Conjugated Systems: Facing Technological Applications. *Macromol. Rapid Commun.* 2007; 28: 1761.

3. Cheng Y-J, Yang S-H and Hsu C-S. Synthesis of Conjugated Polymers for Organic Solar Cell Applications. *Chem. Rev.* 2009; 109: 5868.

4. Groenendaal LB, Jonas F, Freitag D, Harald P and Reynolds JR. Poly(3,4-ethylenedioxythiophene) and Its Derivatives: Past, Present, and Future. *Adv. Mater.* 2000; 12: 481.

5. Turbiez M, re PF, Blanchard P and Roncali J. Mixed p-conjugated oligomers of thiophene and 3,4-ethylenedioxythiophene (EDOT). *Tetrahedron Lett.* 2000; 41: 5521.

6. Raimundo J-M, Blanchard P, Frère P, et al. Push–pull chromophores based on 2,2′-bi(3,4-ethylenedioxythiophene) (BEDOT) π-conjugating spacer. *Tetrahedron Lett.* 2001; 42: 1507.

7. Roncali J, Blanchard P and Frère P. 3,4-Ethylenedioxythiophene (EDOT) as a versatile building block for advanced functional π-conjugated systems. *J. Mater. Chem.* 2005; 15: 1589.

8. Turbiez M, Frère P, Allain M, Videlot C, Ackermann J and Roncali J. Design of organic semiconductors: tuning the electronic properties of pi-conjugated oligothiophenes with the 3,4-ethylenedioxythiophene (EDOT) building block. *Chemistry* 2005; 11: 3742.

9. Mc Lafferty FW and Turecek F. *Interpretation of Mass Spectra, 4th ed.* University Science Books, Sausalito, *CA* (1993).

10. Drahos L and Vékey K. MassKinetics: a theoretical model of mass spectra incorporating physical processes, reaction kinetics and mathematical descriptions. *J. Mass Spectrom.* 2001; 36: 237.

11. Marcus RA and Rice OK. The Kinetics of the Recombination of Methyl Radicals and Iodine Atoms. *J. Phys. Chem.* 1951; 55: 894.

12. Rosenstock HM, Wallenstein MB, Wahrhaftig AL and Eyring H. Absolute Rate Theory for Isolated Systems and the Mass Spectra of Polyatomic Molecules. *Proc. Natl. Acad. Sci. USA* 1952; 38: 667.

13. Beyer T and Swinehart DF. Algorithm 448: Number of Multiply-restricted Partitions. *Commun. ACM.* 1973; 16: 379.

14. Vékey K. Internal Energy Effects in Mass Spectrometry. *J. Mass Spectrom.* 1996; 31: 445.

15. Baer T and Mayer PM. Statistical Rice-Ramsperger-Kassel-Marcus quasiequilibrium theory calculations in mass spectrometry. *J. Am. Soc. Mass Spectrom*. 1997; 8: 103-15.

16. Baer T and Hase WL. *Unimolecular Reaction Dynamics: Theory and Experiments*. Oxford, New York: Oxford University Press, *NY* (1996).

17. Holmes JL, Aubry C and Mayer PM. Proton Affinities of Primary Alkanols: An Appraisal of the Kinetic Method. *J. Phys. Chem. A* 1999; 103: 705-9.

18. Robinson PJ and Holbrook KA. *Unimolecular reactions*. Wiley-Interscience, Chichester, *UK* (1972).

19. Cooks RG, Lester GR, Caprioli RM and Beynon JH. *Metastable ions.* Elsevier Scientific Publishing Campagny, Amsterdam, *NL* (1973).

20. Naban-Maillet J, Lesage D, Bossée A, Gimbert Y, Sztáray J, Vékey K, Tabet JC. Internal energy distribution in electrospray ionization. *J. Mass Spectrom.* 2005; 40: 1.

21. Pak A, Lesage D, Gimbert Y, Vékey K and Tabet J-C. Internal energy distribution of peptides in electrospray ionization : ESI and collision-induced dissociation spectra calculation. *J. Mass Spectrom.* 2008; 43: 447.

22. Rondeau D, Galland N, Zins E-L, Pepe C, Drahos L and Vékey K. Non-thermal internal energy distribution of ions observed in an electrospray source interfaced with a sector mass spectrometer. *J. Mass Spectrom.* 2011; 46: 100.

23. Ichou F, Lesage D, Machuron-Mandard X, Junot C, Cole RB and Tabet J-C. Collision cell pressure effect on CID spectra pattern using triple quadrupole instruments: a RRKM modeling. *J. Mass Spectrom*. 2013; 48: 179.

24. Rondeau D, Drahos L and Vékey K. Internal energy distribution in electrospray ionization: towards the evaluation of a thermal-like distribution from the multiple-collision model. *Rapid Commun. Mass Spectrom.* 2014; 28: 127.

25. Gatineau D, Memboeuf A, Milet A, et al. Experimental bond dissociation energies of benzylpyridinium thermometer ions determined by threshold-CID and RRKM modeling. *Int. J. Mass Spectrom.* 2017; 417: 69.

26. Gömöry Á, Végh P, Sztáray J, Drahos L and Vékey K. Kinetic Energy Release of Protonated Methanol Clusters Using the Low-Temperature Fast-Atom Bombardment: Experiment and Theory Combined. *Eur J Mass Spectrom*. 2004; 10: 213.

27. Drahos L, Sztáray J and Vékey K. Theoretical calculation of isotope effects, kinetic energy release and effective temperatures for alkylamines. *Int. J. Mass Spectrom.* 2003; 225: 233.

28. Nacson S and Harrison AG. Energy transfer in collisional activation. Energy dependence of the fragmentation of n-alkylbenzene molecular ions. Int. J. Mass Spectrom. Ion Process. 1985; 63: 325.

29. Baer T, Dutuit O, Mestdagh H and Rolando C. Dissociation Dynamics of n-Butylbenzene Ions: The Competitive Production of m/z 91 and 92 Fragment Ions. *J. Chem. Phys.* 1988; 92: 5674.

30. Dawson PH. Low-energy collision-activated dissociation of n-butylbenzene. Effect of the electron energy used during parent ion formation. *Int. J. Mass Spectrom. Ion Process.* 1985; 63: 339.

31. Plomley JB, Londry FA and March RE. The Consecutive Fragmentation of n-Butylbenzene in a Quadrupole Ion Trap. *Rapid Commun. Mass Spectrom.* 1996; 10: 200.

32. Muntean F and Armentrout PB. Modeling Kinetic Shifts for Tight Transition States in Threshold Collision-Induced Dissociation. Case Study: Phenol Cation. *J. Phys. Chem. B* 2002; 106: 8117.

33. Beno BR, Wilsey S and Houk KN. The C7H10 Potential Energy Landscape: Concerted Transition States and Diradical Intermediates for the Retro-Diels−Alder Reaction and [1,3] Sigmatropic Shifts of Norbornene. *J. Am. Chem. Soc.* 1999; 121: 4816.

34. Ovcharenko VV, Shaikhutdinov RA, Pihlaja K and Stájer G. Mass-spectrometric differentiation of diexo- and diendo-fused isomers of norbornane/ene-condensed 2-thiouracil and 1,3-thiazino[3,2-a]pyrimidine derivatives: stereoselectivity of retro-diels-alder fragmentations under EI and CI conditions. J. *Am. Soc. Mass Spectrom.* 2001; 12: 1011.

35. Lim H, Schultz DG, Gislason EA and Hanley L. Activation Energies for the Fragmentation of Thiophene Ions by Surface-Induced Dissociation. *J. Phys. Chem.* B 1998; 102: 9362.

[i] Gaussian 09, Revision **D.01**, M. J. Frisch, G. W. Trucks, H. B. Schlegel, G. E. Scuseria, M. A. Robb, J. R. Cheeseman, G. Scalmani, V. Barone, B. Mennucci, G. A. Petersson, H. Nakatsuji, M. Caricato, X. Li, H. P. Hratchian, A. F. Izmaylov, J. Bloino, G. Zheng, J. L. Sonnenberg, M. Hada, M. Ehara, K. Toyota, R. Fukuda, J. Hasegawa, M. Ishida, T. Nakajima, Y. Honda, O. Kitao, H. Nakai, T. Vreven, J. A. Montgomery, Jr., J. E. Peralta, F. Ogliaro, M. Bearpark, J. J. Heyd, E. Brothers, K. N. Kudin, V. N. Staroverov, R. Kobayashi, J. Normand, K. Raghavachari, A. Rendell, J. C. Burant, S. S. Iyengar, J. Tomasi, M. Cossi, N. Rega, J. M. Millam, M. Klene, J. E. Knox, J. B. Cross, V. Bakken, C. Adamo, J. Jaramillo, R. Gomperts, R. E. Stratmann, O. Yazyev, A. J. Austin, R. Cammi, C. Pomelli, J. W. Ochterski, R. L. Martin, K. Morokuma, V. G.

Zakrzewski, G. A. Voth, P. Salvador, J. J. Dannenberg, S. Dapprich, A. D. Daniels, Ö. Farkas, J. B. Foresman, J. V. Ortiz, J. Cioslowski, and D. J. Fox, Gaussian, Inc., Wallingford CT, 2009.

[ii] P. J. Stephens, F. J. Devlin, C. F. Chablowski, and M. Frisch, *J. Phys. Chem*. 1994; 98 : 11623, and refs therein

[iii] W.J. Hehre, R. Ditchfield, J. A. Pople, *J. Chem. Phys*. 1972; 56, 2257.